ISSN 1028-334X, Doklady Earth Sciences, 2006, Vol. 408, No. 4, pp. 590–594. © Pleiades Publishing, Inc., 2006.
Original Russian Text © D.D. Gordienko, Yu.F. Kopnichev, I.N. Sokolova, 2006, published in Doklady Akademii Nauk, 2006, Vol. 408, No. 2, pp. 238–242.

GEOPHYSICS

Spatiotemporal Variations of Short-Period *S*-Wave Attenuation Field in Source Zones of Large and Great Earthquakes

D. D. Gordienko[a], Yu.F. Kopnichev[b], I.N. Sokolova[b]

Presented by Academician V.N. Strakhov September 2, 2005

Received September 9, 2005

DOI: 10.1134/S1028334X06040180

Attenuation field characteristics of shear waves in upper mantle in source zones of 34 large and great earthquakes worldwide were studied. Effective coda quality factor of *Lg* and *Sn* waves in two time intervals were determined. It is demonstrated that the period of 20 to 25 years following a large earthquake shows a regular decrease in attenuation in the uppermost mantle. This trend is most evident for events with normal and strike-slip faulting mechanisms. The revealed phenomena are attributed to ascent of mantle fluids into the crust following violent earthquakes.

Short-period shear waves are most sensitive to the presence of the liquid phase. Therefore, their characteristics can be used to study the processes of fluid migration in the crust and uppermost mantle [1–4]. This paper examines spatiotemporal variations of *S*-wave attenuation field in source zones of 34 large and great earthquakes (maximum hypocenter depth 60 km) that occurred worldwide in the period 1897–2003 (M_S = 7.0–8.6, table [5, 6]). Moreover, for the sake of comparison, attenuation field characteristics were studied in regions (primarily, Central Asia and North America) with no strong earthquakes ($M \geq 6.5$) since 1900.

We processed seismograms of over 350 shallow earthquakes recorded by 42 digital and analog stations located ~300–600 km from epicenters. Attenuation field heterogeneities are most prominent at frequencies close to 1 Hz [1, 2, 7]. Therefore, we performed the preliminary frequency filtration of the recordings using a filter (central frequency = 1.25 Hz, pass bandwidth = 2/3 octave at 0.7 maximum level) similar to the respective ChISS-filter [8].

Envelopes of *Lg* and *Sn* coda of recordings of relatively small earthquakes (generally, $M < 5.5$) were examined. As shown in [8–10], at a frequency of ~1 Hz, the coda of both *Lg* and *Sn* waves is formed principally by *S*-waves reflected from numerous subhorizontal boundaries in the upper mantle. With increasing time *t* from the start of emission, the coda meets waves falling on boundary *M* more and more steeply and penetrating greater depths in the upper mantle. Figure 1 provides a simplified scheme of propagation of rays forming *Lg* and *Sn* coda. Ray I is the head wave propagating along the boundary M. The later *S*-waves are reflected from various boundaries in the upper mantle. If the source zone in the upper mantle incorporates an area of relatively weak (strong) attenuation, this will result in a relatively slow (quick) amplitude attenuation in the initial part of the coda (rays II and III). Ray III is followed by *S*-waves penetrating the zone of "normal" (for the given depth range) attenuation. This ensures either an abrupt

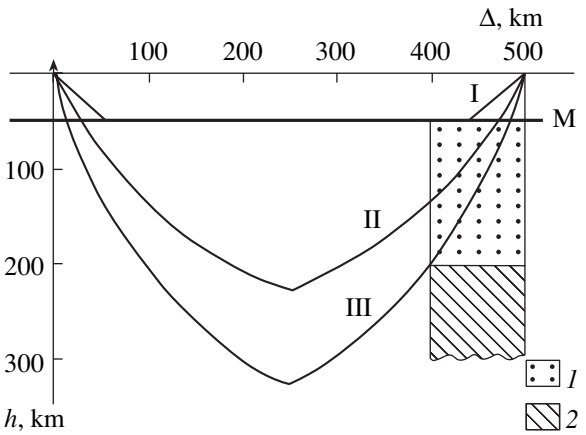

Fig. 1. Scheme of propagation of rays forming *Lg* and *Sn* coda. (*1*) The uppermost mantle area of an abrupt attenuation shift in time; (*2*) the "normal" attenuation area.

[a] *Shmidt Institute of Physics of the Earth, Russian Academy of Sciences, ul. Bol'shaya Gruzinskaya 10, Moscow, 123995 Russia*

[b] *Institute of Geophysical Research, National Nuclear Center, Almaty oblast, Talger, Kazakhstan*

Q_1 and Q_2 values for various source zones

Region	Date	φ	λ	M_S	Mechanism	Q_1	Q_2	Station
		Degree						
Himalayas	June 12, 1897	26	91	>8	thrust	200	310	LSA
Tien Shan	Aug. 22, 1902	39.8	76.2	7.6	reverse faulting	590	790	TLG
Tien Shan	Jan. 3, 1911	42.8	77.3	7.7	reverse faulting	670	790	MAKZ
Tibet	Dec. 16, 1920	36.62	105.40	8.4	oblique-reverse faulting	740	420	XAN
Japan	Mar. 2, 1933	39.25	144.5	8.3	normal faulting	1300	1150	ERM
Himalayas	Jan. 15, 1934	27.55	87.09	8.1	thrust	330	510	LSA
Indonesia	Dec. 28, 1935	0.00	98.25	7.5	strike-slip	270	270	BTDF
Japan	Dec. 7, 1944	33.75	136.00	7.8	thrust	300	390	MAJO
Himalayas	Aug. 15, 1950	28.70	96.60	8.6	strike-slip	840	340	LSA
California	July 21, 1952	35.00	–119.00	7.8	oblique-reverse faulting	410	300	MNV
Japan	Nov. 25, 1953	34.00	141.50	7.9	normal faulting	1100	440	MAJO
Baikal region	June 27, 1957	56.20	116.59	7.6	oblique-normal faulting	1700	710	BDN
Mongolia	Dec. 4, 1957	45.31	99.21	8.0	oblique-reverse faulting	540	740	ULN
Nevada	Aug. 18, 1959	44.70	–110.80	7.5	normal faulting	540	570	DUG
Chile	May 22, 1960	–38.20	–73.50	8.5	thrust	340	510	PLCA
Alaska	Mar. 28, 1964	61.10	–147.60	8.4	thrust	310	360	COLA
Chile	Dec. 28, 1966	–25.50	–70.70	7.7	thrust	250	370	LCO
Tien Shan	Aug. 11, 1974	39.39	73.86	7.2	oblique-reverse faulting	350	420	GAR
Indonesia	Aug. 19, 1977	–11.09	118.46	8.1	normal faulting	1300	410	KAPI
Tien Shan	Mar. 24, 1978	42.9	78.70	7.0	oblique-reverse faulting	490	740	MAKZ
Chile	Mar. 3, 1985	–33.13	–71.87	7.8	thrust	290	490	LCO
Mexico	Sep. 19, 1985	18.14	–102.71	8.1	thrust	200	350	UNM
California	June 28, 1992	34.18	–116.51	7.6	strike-slip	380	310	MNV
Tien Shan	Aug. 19, 1992	42.10	73.60	7.3	reverse faulting	270	630	AML
Kuril Islands	Oct. 4, 1994	43.77	147.32	8.3	oblique-reverse faulting	200	530	ERM
Indonesia	Jan. 1, 1996	0.73	119.93	7.9	oblique-reverse faulting	260	510	KAPI
Tibet	Nov. 8, 1997	35.07	87.32	7.9	strike-slip	120	320	LSA
Kamchatka	Dec. 5, 1997	54.84	162.04	7.6	reverse faulting	210	420	PET
Turkey	Aug. 17, 1999	40.75	29.86	7.7	strike-slip	200	370	ANTO
Mexico	Sept. 30, 1999	16.6	–96.93	7.5	reverse faulting	220	320	UNM
Salvador	Jan. 13, 2001	13.05	–88.66	7.8	reverse faulting	120	330	JTS
Peru	June 23, 2001	–16.26	–73.64	8.2	reverse faulting	150	360	NNA
Alaska	Nov. 3, 2002	63.52	–147.44	8.0	strike-slip	310	390	COLA
Altai	Sept. 27, 2003	50.04	87.81	7.3	strike-slip	290	740	MKAR

increase or decrease of attenuation speed of coda amplitudes.

Formula $A_c(t) \sim t^{-1}\exp\left(-\frac{\pi t}{Q_S T}\right)$ (T is the oscillation period, t is the lapse time [8]) was used to determine the effective quality factor in two coda intervals. The first interval immediately follows group *Lg* 70 s long (mainly t = 180–250 s). The second interval is marked at t = 250–400 s (for brevity sake, let us designate them as Q_1 and Q_2, respectively). Simple estimates show that for epicentral distance Δ = 500 km with ray drift of ~100 km, *S*-waves in the coda penetrate to ~140 km at t = 180 s and to 210 km depth at t = 250 s.

Figure 2 shows samples of coda envelopes of recordings of earthquakes in relatively short time intervals ΔT (up to 5 yr) following four large earthquakes worldwide. The earthquakes had different types of faultings in the source. Figure 2 evidences a relatively greater slope at the coda onset for all the envelopes. The

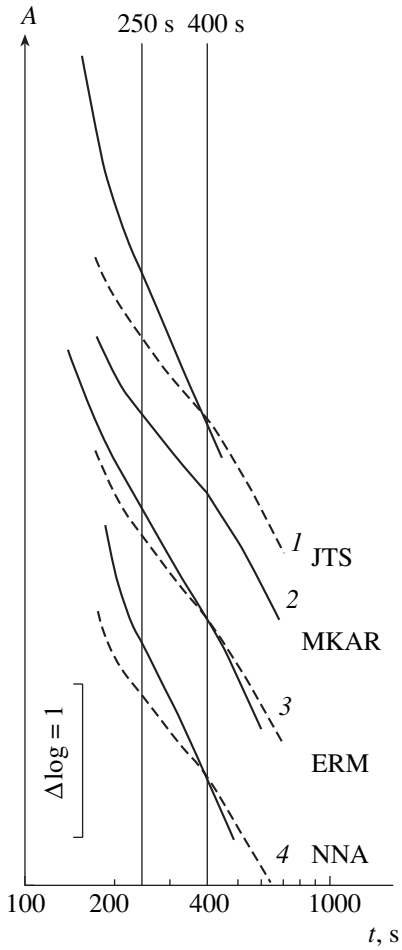

Fig. 2. Envelopes of recordings of aftershocks and earthquakes occurring with $\Delta T > 5$ yr following large earthquakes. (*1*) Salvador, 2001 (normal faulting); (*2*) Altai, 2003 (strike-slip faulting); (*3*) Shikotan (Kuril Islands), 1994 (oblique-reverse faulting); (*4*) Peru, 2001 (thrust). Dashed line corresponds to the Altai earthquake envelope. Here and in Fig. 3, abbreviations designate stations.

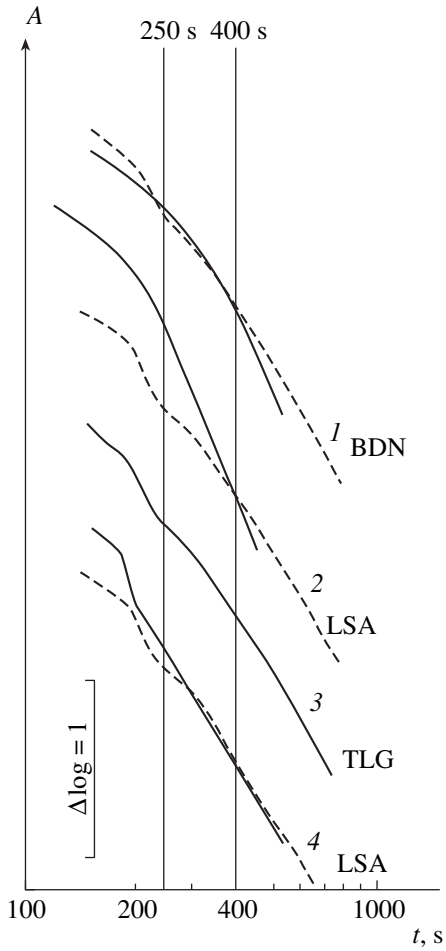

Fig. 3. Envelopes of recordings of local events in source zones of large and great earthquakes with $\Delta T > 17$ yr. (*1*) Muya, Baikal region, 1957 (oblique-normal faulting); (*2*) Assam, Himalayas, 1950 (strike-slip faulting); (*3*) Kashgar, Tien Shan, 1902 (reverse faulting); (*4*) Bihar–Nepal Himalayas, 1934 (thrust). Dashed line corresponds to the Kashgar earthquake envelope.

slope abruptly decreases at the 250–400 s interval. A completely different situation was observed in areas where the examined events occurred after long time spans following large and great earthquakes. Figure 3 provides instances of coda envelopes for source zones of other four large earthquakes with different types of faultings. These envelopes were drawn from recordings made 17–96 years following these events. It can be seen that in all the instances the initial coda amplitudes fade out much less than in Fig. 2. The weakest attenuation of coda corresponds to events with mechanisms of the oblique-normal and strike-slip types.

The table shows variations of Q_1 values for various source zones within 120–1700, whereas the variation range of Q_2 is much less (270–1150). The lesser spread for Q_2 values does not contradict the existing notions of the decrease of upper mantle heterogeneity with depth [8]. The maximum Q_1 values (740–1700) were obtained for the source zones of the following earthquakes: Hi Yuan (1920), Sanriku Oki (1933), Assam (1950), Boso Oki (1953), Muya (1957), and Sumba (1977).

Figure 4 shows the $\frac{Q_1}{Q_2}$ ratio as a function of time ΔT. For comparison sake, the data scatter band ($\pm\sigma$) is provided for 44 paths recorded in various regions worldwide where no large earthquakes ($M > 6.5$) were recorded since 1900 (some areas of Kopet Dagh, Kazakh Platform, Tien Shan, Pakistan, Tibet, Mongolia, Baikal region, and western and eastern United States). According to data obtained from recordings of 26 stations, the average of $\frac{Q_1}{Q_2}$ values for these paths is 0.45 ± 0.1 (with Q_1 and Q_2 values varying within 145–540 and 290–980, respectively). It should be noted that

in this case the maximum Q_1 values are approximately three times lower than those for the studied source zones.

Figure 4 evidences that for aftershocks in the first year following strong earthquakes, $\frac{Q_1}{Q_2}$ values are restricted to the above band. At longer ΔT, one can observe a sharp distinction in values of the studied parameter for different mechanism types. For normal and strike-slip faulting, $\frac{Q_1}{Q_2}$ values very rapidly grow for 20–25 years to 2.4–3.2, which is far beyond the limits of the 15σ interval. At $\Delta T > 25$ yr, we see a decreasing trend of the average $\frac{Q_1}{Q_2}$ value for such faulting types. For reverse faulting and thrusts, the $\frac{Q_1}{Q_2}$ parameter grows much slower and varies within a relatively narrow range of 0.65–0.86 (at 2–4σ level) at $\Delta T > 25$ yr. For oblique-reverse faultings, $\frac{Q_1}{Q_2}$ values are intermediate between the "pure" reverse faulting and strike-slip faulting. The primary correlation between $\frac{Q_1}{Q_2}$ and ΔT is mainly related to the abrupt shift of the Q_1 value (table). The highest $\frac{Q_1}{Q_2}$ values correspond to source zones of earthquakes that show very high Q_1 values. One can see a distinct correlation of the maximum Q_1 values with the focal mechanism. The highest Q_1 values were obtained for normal and oblique-normal faulting (up to 1100–1700), up to 740–840 for strike-slip faulting and oblique-reverse faultings, up to 590–670 for reverse faulting, and up to 330–340 for thrusts.

The data obtained show that Q_1 values in normal conditions (beyond source zones), as well as immediately after large earthquakes, vary within a relatively narrow range. This indicates a noticeable decrease of *S*-wave attenuation in the upper mantle with depth. At the same time, source zones of large and great earthquakes worldwide are characterized by anomalously high Q_1 and $\frac{Q_1}{Q_2}$ values in the 15–20 years following these events. This corresponds to a sharp decrease of *S*-wave attenuation in the upper mantle at a depth of ~200 km.

The increase of Q value of shear waves in the uppermost mantle in a rather short (in the geologic time scale) period can only be related to fluid migration processes. Results of the analysis show that large and great earthquakes are followed by the ascent of fluids from the upper mantle into the crust. This is consistent with our previous conclusions made from the analysis of the

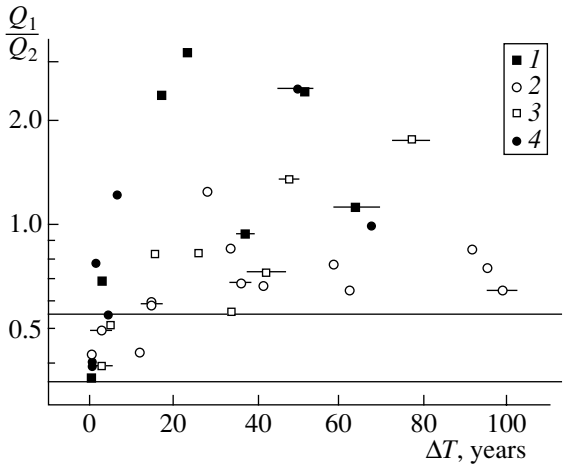

Fig. 4. The dependence of $\frac{Q_1}{Q_2}$ values from time ΔT after a large earthquake. Horizontal band corresponds to (±σ) area boundaries for regions with no $M \geq 6.5$ events since 1900. Earthquake mechanisms: (*1*) normal and oblique-normal faulting; (*2*) reverse faulting and thrusts; (*3*) oblique-reverse faultings; (*4*) strike-slip faulting. Horizontal marks correspond to time intervals (otherwise they do not exceed the symbol size).

S-wave attenuation field on the basis of local earthquake coda in Tien Shan [2], as well as the study of the temporal variations of the V_p/V_s ratio in the source zone of the Antofagasta earthquake in 1995 (Northern Chile, $M = 8.0$) [3, 4]. This is also evidenced by a very strong attenuation of *Lg* waves in the crust within large earthquake zones of Tien Shan established on the basis of recordings of underground nuclear explosions at the Semipalatinsk test site [11]. Rise of juvenile fluids is also evidenced by the presence of mantle helium isotopes in source zones and their neighborhoods [2]. At the same time, this work is the first to show the considerable dependence of the ascent speed of mantle fluids from the focal mechanism.

Anomalously high Q_1 and $\frac{Q_1}{Q_2}$ values for the greatest normal and strike-slip faulting (as compared to reverse faulting and thrusts) agree with the conclusion of huge quantities of water pouring out on the surface after large earthquakes with such faultings [12]. This phenomenon is most probably related to a very high permeability of rocks in such areas, relative to normal faulting, strike-slip faulting, and oblique-reverse faulting events are characterized by a relatively lesser development of local extension zones (coulisses), which apparently serve as the main conduit for the rising mantle fluids [13]. At the same time, in compression zones responsible for reverse faulting and thrusts, permeability of rocks for earthquakes of commensurable energy must be much lower (especially for thrusts), resulting in a much lower degree of the uppermost mantle "draining."

The results obtained can be used for long-term earthquake forecasts since large seismic events are presumably most probable in regions of relatively high *S*-wave attenuation in the uppermost mantle (low $\frac{Q_1}{Q_2}$ values).

ACKNOWLEDGMENTS

We are grateful to the IRIS research consortium for providing the GSN data [14].

REFERENCES

1. Yu. F. Kopnichev and I. N. Sokolova, Fiz. Zemli, No. 11, 73 (2001).
2. Yu. F. Kopnichev and I. N. Sokolova, Fiz. Zemli, No.7, 35 (2003).
3. S. Husen and E. Kissling, Geology **29**, 847 (2001).
4. A. Koerner, E. Kissling, and S. Miller, J. Geophys. Res. **109**, No.B6. DOI 10.10291/2003JB002816 (2004).
5. J. Pacheco and L. Sykes, Bull. Seismol. Soc. Am. **82**, 1306 (1992).
6. W.-P. Chen and P. Molnar, J. Geophys. Res. **82**, 2945 (1997).
7. O. I. Aptikaeva and Yu. F. Kopnichev, J. Earthquake Predict. Res. **2**, 497 (1993).
8. Yu. F. Kopnichev, *Short-Period Seismic Wave Field* (Nauka, Moscow, 1985) [in Russian].
9. Yu. F. Kopnichev and A. R. Arakelian, Vulkanol. Seimol., No. 4, 77 (1988).
10. P. B. Kaazik, Yu. F. Kopnichev, I. L. Nerserov, and M. Kh. Rakhmatullin, Fiz. Zemli, No.4, 38 (1990).
11. Yu. F. Kopnichev and I. N. Sokolova, Dokl. Nauk **395**, 818 (2004) [Dokl. Earth Sci. **395**, 461 (2004)].
12. R. Muir-Wood and G. King, J. Geophys. Res. **98**, 22035 (1993).
13. O.I. Aptikaeva, S.S. Aref'ev, S.I. Kvetinskii, et al., Dokl. Akad. Nauk **344**, 533 (1995).
14. R. Butler, T. Lay, K. Creager, et al., Eos Trans. **85**, 225 (2004).